C. R. Mecanique 342 (2014) 356–362

Contents lists available at ScienceDirect

Comptes Rendus Mecanique

www.sciencedirect.com

Separation flow control

Salient and smooth edge ramps inducing turbulent boundary layer separation: Flow characterization for control perspective

Antoine Debien *, Sandrine Aubrun, Nicolas Mazellier, Azeddine Kourta

Université d'Orléans, ENSI de Bourges, PRISME, EA 4229, 8, rue Léonard-de-Vinci, 45072 Orléans cedex 2, France

ARTICLE INFO

Article history:
Received 6 September 2013
Accepted 21 November 2013
Available online 3 June 2014

Keywords:
Separation
Ramp
Experiment

ABSTRACT

Turbulent boundary layer separation induced by a salient ramp and a smooth-edge one are characterized. Upstream from the separation point, the momentum thickness Reynolds number $Re_\theta \approx 3500$. Pressure distribution and gradient pressure distribution are analyzed on the overall model. Upstream from the ramp, boundary layer is characterized using hot-wire anemometry. Recirculation zone and unsteady behavior of separation point are evaluated using a PIV system. The shear layer roll-up and vortex shedding times scales obtained with cross hot-wire anemometry show good agreements with the literature. This study is a step toward the development of a robust control strategy undertaken in the frame of the ANR SePaCode project (2011–2014).

1. Introduction

Turbulent boundary layer (TBL) separation occurs in many industrial processes. It produces detrimental effects as drag increase, lift reduction, and pressure loss, which can lead to the inefficiency of the vehicle or of industrial designs.

The physical mechanism responsible for flow separation is well known: under the influence of an adverse pressure gradient, the flow near the wall decelerates until separation, inducing the development of a shear layer that transports vorticity far from the wall. Occurring when wall shear stress falls to zero, the position of the TBL detachment with adverse pressure gradient has an unsteady behavior. Thus position of the TBL separation has to be characterized, including transitory detachment properties [1]. Downstream from the separation point, the flow is highly dependent on upstream conditions. It is characterized by a shear layer where turbulence production is diffused by large eddy structures in the backflow near the wall, where negligible turbulence energy production occurs [2–4]. During the shear layer development process, instabilities induce the emergence of dominant coherent structures [5,6]. Roll-up of the shear layer induced by the Kelvin–Helmholtz instability is scaled by a Strouhal number $St_\theta = 0.012$ obtained using the momentum thickness θ of the boundary at the mean separation point [7,8]. As shear layer develops, progressive merging of structures will decrease the time scale and lead to a second dominant scale, the shedding mode. Based on the separation length, the shedding mode is characterized by a Strouhal number $St_{L_{sep}} = 0.6–0.8$ [9–11].

Flow control appears as a solution to delete or reduce the separation and had received special attention in the last decades [10,12–14], highlighting the need for using a flow-control strategy based on natural flow instabilities and dominant flow structures [15,16]. In this context, the SePaCoDe ANR project (2011–2014) aims to propose a robust model-based separation control strategy leading to 2D separations occurring on salient and smooth-edge ramps. Furthermore, robustness of control implies a good comprehension of the predominant phenomena in the separation process [17].

* Corresponding author.
E-mail address: antoine.debien@univ-orleans.fr (A. Debien).

http://dx.doi.org/10.1016/j.crme.2014.05.003
1631-0721/

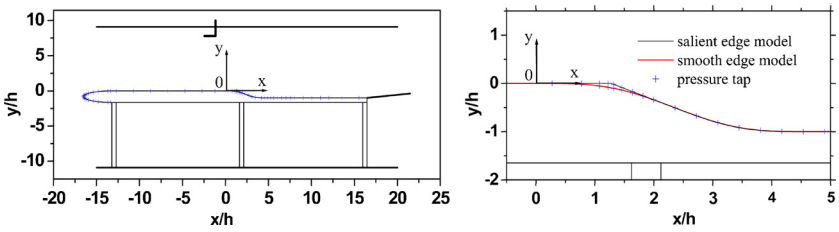

Fig. 1. (Color online.) Experimental facility and detail of smooth and salient edge ramps.

It is then the goal of the present study to describe the turbulent separation occurring on salient and smooth edges through wind tunnel experiments conducted at PRISME Laboratory. Wall-pressure measurement and boundary layer characterization with hot-wire anemometry are conducted to characterize the flow upstream from separation, while Particle Image Velocimetry (PIV) and cross hot wire are used to characterize the separation region.

2. Experimental setup

2.1. Wind-tunnel and ramp facilities

Experiments are conducted in the subsonic Malavard wind tunnel of PRISME Laboratory. In the test section—$5 \times 2 \times 2$ m^3 (length $\times$ width $\times$ height)—, up to a 60 m/s free-stream velocity can be achieved, with a residual turbulence intensity lower than 0.4%. The ramp model (Fig. 1) is set at the middle height of the test section and spans the tunnel width. It is comprised of four parts: a leading edge with elliptic profile, a flat plate where TBL develops, the ramp and a second flat plate downstream from the ramp. Furthermore, a flap is fixed at the trailing edge to ensure symmetrical pressure distribution at the leading edge (the flap is set at $\alpha = -7°$ incidence). Two models of ramp (length $l = 470$ mm) with a step height $h = 100$ mm have be used (Fig. 1): a salient edge ramp (edge located at $x/h = 1.27$) with a slant angle of 25° ending with a 7 order polynomial (Eq. (1), $0.5 \leq x/l \leq 1$) and a smooth edge ramp with a curvature defined by a 7 order polynomial and a maximal slant angle of 25° (Eq. (1)).

$$\frac{y}{h} = 1 - 35\left(\frac{x}{l}\right)^4 + 84\left(\frac{x}{l}\right)^5 - 70\left(\frac{x}{l}\right)^6 + 20\left(\frac{x}{l}\right)^7, \quad 0 \leq x \leq l \tag{1}$$

For all results presented here, free-stream velocity is set at $U_0 = 20$ m/s, achieving a Reynolds number $\mathrm{Re}_\theta \approx 3500$ based on the momentum thickness upstream from the separation point. The boundary layer is tripped to fix the transition, thus warranting the reproducibility of its properties during the overall experiments. Based on displacement thickness assessment, a zigzag tripper of 300 µm thickness is placed 103 mm downstream from the leading edge [18].

2.2. Pressure probe measurements

To characterize the pressure distribution on the model, wall pressure taps (0.3 mm in diameter) are connected to pressure sensors by a 1.50 m-long tygon capillary. A PSI 8400 (2500 Pa, ± 0.75 Pa) acquisition unit allows the measurement of 112 pressure transducers. Time-series of fluctuations pressure are acquired with a 100 Hz sampling frequency. The recording time is $40{,}960U_0/h$. The pressure coefficient ($C_p = \frac{P-P_0}{\frac{1}{2}\rho U_0}$) and the gradient pressure coefficient are deduced with uncertainty estimates of $\pm 1.7\%$ and $\pm 5\%$, respectively.

2.3. Single hot-wire measurements

TBL properties upstream from the separation point are characterized with single hot wire anemometry. The data acquisition system was manufactured by Dantec. The probe (55P11) is made of a 5 µm-diameter wire 1.25 mm in length, which corresponds to $\frac{l}{\eta} = 43$. Calibration of the hot-wire probe is performed with a Dantec 90H02 Flow Unit. A fourth-order polynomial fits the calibration curve through the data points. Hot-wire profiles are obtained with 50 points. The statistic properties of velocity are obtained at a 60 kHz sampling frequency (cut-off frequency of 30 kHz, which is about twice the Kolmogorov frequency) with an acquisition time $28{,}000 < T_{\mathrm{aq}} U_{\mathrm{e}}/\delta < 120{,}000$.

Based on a work by Alfredsson and Orlu [19], the validation of near-wall measurements is done using data sampling diagnostic according to the $u' = f(u)$ curve, which is characterized by a linear profile as velocity vanishes. Then the probe position and the friction velocity are estimated according to $u^+ = 14.5 \tanh(y^+/14.5)$ for $4 < u^+ < 11$ [20].

2.4. Cross-wire measurement

Downstream from the separation point, the instantaneous characteristics of the shear layer are performed with a cross-wire anemometer. The 55P61 probe used for measurement is composed of two 5 µm wires 1.25 mm in length arranged in

X-arrays. Velocity calibration is conducted in the same way as single hot-wire calibration. Angular calibration is performed from $\beta = -45°$ to 45° with a 5° discretization. Time-series are acquired at a 30 kHz frequency (cut-off frequency of 10 kHz). The recording time is $26{,}000U_0/h$.

2.5. Particule Image Velocimetry

The flow field over the ramp is obtained with a TSI Particle Image Velocimetry (PIV) system using two overlapping planes acquired by two CCD cameras (TSI PowerView plus 4M 2048 × 2048 pixels^2). The two cameras and the Nd–Yag Quantel laser (Big Sky Laser, 150 mJ) are driven by a TSI Synchro Laser Pulse (610035). The use of 50 mm lenses (AF D Nikkor, f 1:1.8) allows a velocity field of 390×390 mm^2 for each camera, leading to a global velocity field of 700×390 mm^2. Velocity fields are computed from images by a multipass algorithm with a first pass of 32×32 pixels^2 and a second pass of 16×16 pixels^2 (overlap 50%) using the TSI software. This process achieves a vector velocity each 1.5 mm. A total of 3400 samples are acquired to obtain the statistical properties of the velocity field. The statistical errors of the mean and second-order moments are respectively 1% and 3% for a 97% confidence interval [21].

3. Results and discussion

3.1. Salient edge experiments

The pressure coefficient distribution along the streamwise direction is showed in Fig. 2. Due to the acceleration imposed by the elliptic profile, C_p drop until it reaches a minimum at $x/h = -14.8$. It then grows up and remains roughly constant over the range $-8.7 < x/h < -4.7$, where the pressure gradient $\frac{dC_p}{dx}$ reaches its minimum. Beyond $x/h > -4.7$, TBL undergoes a favorable pressure gradient as the flow approaches the ramp. From the leading edge, the pressure coefficient decreases up to a suction peak ($x/h = -14.8$) induced by flow acceleration. Then the pressure coefficient vanishes ($C_p < 0.01$) for $-8.7 < x/h < -4.7$ and presents a minimal value of the pressure gradient ($-7.7 < x/h < 3.7$, $|\frac{dC_p}{dx}| < 0.044$ m^{-1}). For $x/h > -4.7$, favorable pressure gradient occurs as flow approaches the ramp. Downstream from the salient edge, a constant plateau $C_p = -0.07$ up to $x/h = 4.7$ is induced by the presence of a recirculation zone. Then the pressure coefficient increases up to a value $C_p = 0.2$ at $x/h = 9.04$ and converges downstream toward a value $C_p = 0.19$.

Fig. 3 shows the dimensionless profiles of the mean and fluctuating streamwise velocity measured with hot-wire probe upstream from the salient edge. Due to the favorable pressure gradient, the boundary layer thickness and the shape factor decrease up to the salient edge (Table 1). At the salient edge, the boundary layer thickness is about 22 mm and the

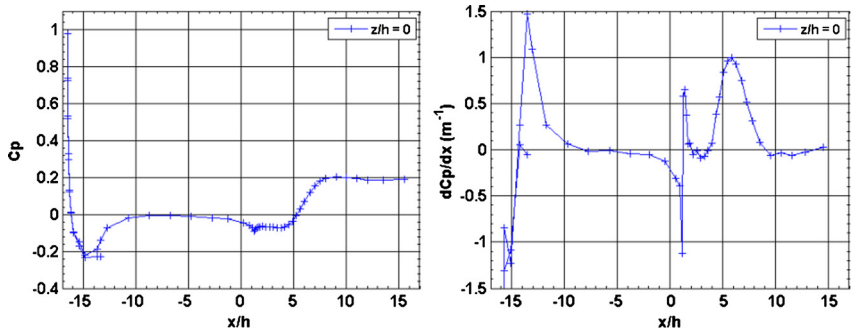

Fig. 2. (Color online.) Pressure coefficient and pressure gradient distribution along the ramp model.

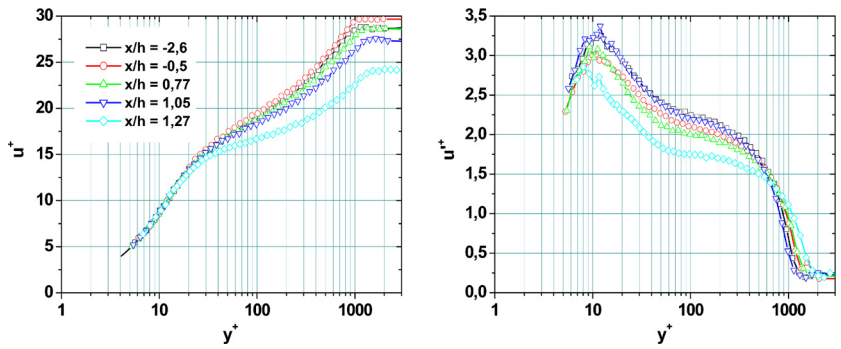

Fig. 3. (Color online.) Profiles of the mean streamwise velocity and rms velocity u'^+ in inner scaling.

Table 1
Turbulent boundary layer characteristics.

x/h	−2.6	−0.5	0.77	1.05	1.27
U_e (m/s)	19.50	19.48	19.96	20.12	21.77
δ_{99} (mm)	∼21.98	∼21.92	∼21.95	∼25.26	∼22.01
δ^* (mm)	3.63	3.73	3.89	3.88	3.35
δ_θ (mm)	2.65	2.72	2.86	2.93	2.6
Re_θ	3312	3406	3662	3778	3628
H_{12}	1.37	1.37	1.36	1.32	1.28
u_τ (m/s)	0.674	0.657	0.697	0.729	0.90
τ_w (kg/m·s^2)	0.54	0.513	0.577	0.633	0.96

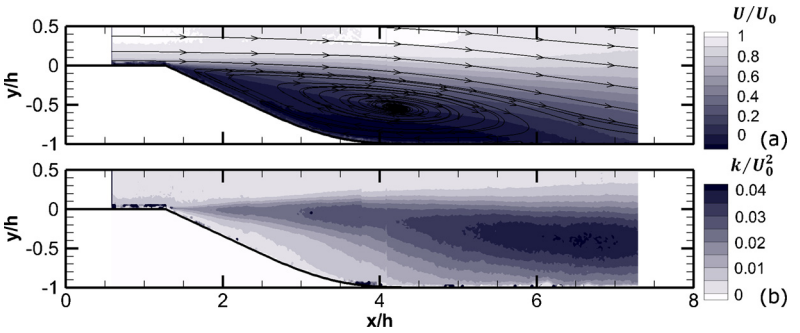

Fig. 4. Mean streamwise velocity over the ramp and Turbulent Kinetic Energy (TKE).

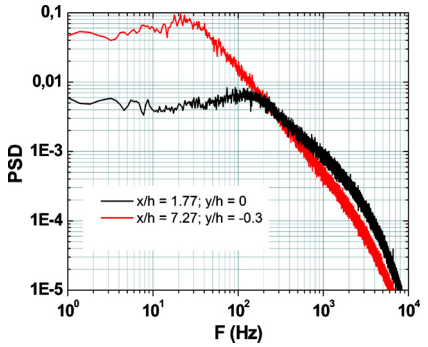

Fig. 5. (Color online.) PSD of transverse velocity component obtained in the shear layer near separation point ($x/h = 1.77$) and in the wake flow ($x/h = 7.27$).

momentum thickness equals 2.6 mm, which corresponds to a Reynolds number $\mathrm{Re}_\theta = 3628$. The location of the near-wall turbulence peak of rms streamwise velocity profiles (Fig. 3) ranges between $y^+ \approx 8$ and $y^+ \approx 12$.

The mean stream-wise velocity field computed from PIV (Fig. 4a) evidences a mean separation point occurring slightly downstream from the salient edge, at $x/h = 1.27$. Downstream from the separation point, a shear layer progressively develops above a mean recirculation zone (Fig. 4a). The mean center of the recirculation zone is located at $\{x/h = 4.2; y/h = -0.54\}$, and the reattachment point of recirculation is located at $x/h = 6.57$, yielding a separation length $L_{\mathrm{sep}} = 5.3h$. The maximum levels of the turbulent kinetic energy (TKE, Fig. 4b) are present in shear layer [4]. The TKE value at the separation point is $k/U_0^2 = 0.015$. This value progressively increases up to a maximal value $k/U_0^2 = 0.04$ achieved above the end of the recirculation zone ($6.19 < x/h < 7$ and $y/h = 0.39$).

The shear layer roll-up and vortex shedding frequencies are emphasized by Power Spectral Density (PSD) of the transverse velocity component for two positions (Fig. 5): the first one in a shear layer near separation point ($x/h = 1.77$) and the second in the wake flow ($x/h = 7.27$). Close to the separation point, the PSD exhibits a shear layer roll-up frequency of 110 Hz, corresponding to a Strouhal number $\mathrm{St}_\theta = 0.014$, while in the wake, a shedding frequency of 20–25 Hz is observed, which gives a Strouhal number $\mathrm{St}_{L_{\mathrm{sep}}} = 0.53$–$0.66$, consistent with the literature [7–11].

3.2. Smooth edge experiments

Fig. 6 displays the pressure coefficient distribution along the model. A minimal amplitude of $C_p = -0.013$ is achieved at $x/h = -8.7$. In the range $-7.7 < x/h < -5.7$, a minimal value of $\frac{\mathrm{d}C_p}{\mathrm{d}x} = -0.035\ \mathrm{m}^{-1}$ occurs. For $x/h > -5.7$, a strong favorable pressure gradient appears up to $x/h = 1.07$. Then flow expansion induces pressure coefficient increase up to

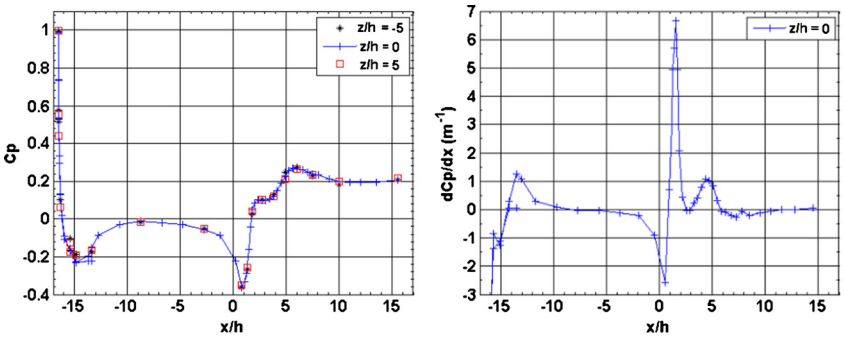

Fig. 6. (Color online.) Pressure coefficient and pressure gradient distribution along the ramp model.

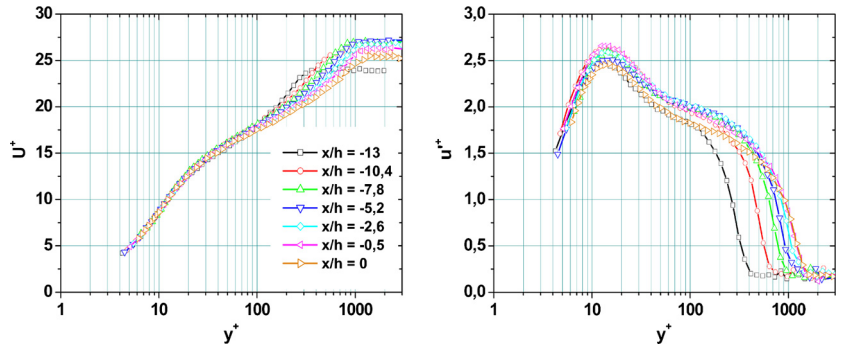

Fig. 7. (Color online.) Profiles of the mean streamwise velocity and rms velocity in inner scaling.

Table 2
Turbulent boundary layer characteristics.

x/h	−13	−10.4	−7.8	−5.2	−2.6	−0.5	0
U_e (m/s)	21.55	20.09	20.32	20.08	20.25	20.65	21.25
δ_{99} (mm)	∼6.17	∼12.47	∼14.44	∼19.04	∼18.95	∼21.95	∼21.94
δ^* (mm)	1.08	1.97	2.66	3.18	3.38	3.34	3.08
δ_θ (mm)	0.75	1.41	1.92	2.32	2.48	2.51	2.37
Re_θ	1011	1815	2506	2981	3235	3327	3223
H_{12}	1.44	1.4	1.385	1.37	1.363	1.33	1.3
u_τ (m/s)	0.875	0.769	0.75	0.739	0.755	0.783	0.833
τ_w (kg/m·s^2)	0.911	0.704	0.67	0.649	0.678	0.73	0.826

separation point where a pressure plateau occurs ($2.36 < x/h < 3.45$). From $x/h > 3.45$, the pressure coefficient increases up to a local maximum ($x/h = 5.6$) and decreases downstream to a value $C_p = 0.2$ achieved for $x/h > 10$.

The TBL evolution upstream from the ramp is displayed in Fig. 7 for seven positions. Beyond $x/h = -5.7$, the displacement thickness and the shape factor decrease (Table 2) as a favorable pressure gradient occurs (Table 2). The boundary layer thickness does not decrease before $x/h = -0.5$, which can be explained by the low favorable pressure gradient and the bias induced by the boundary layer's thickness detection. All rms streamwise velocity profiles (Fig. 7) collapse for $5 < y^+ < 30$, with a near-wall turbulence peak at $y^+ = 14$. At $x/h = 0$, the boundary layer presents a thickness $\delta \approx 22$ mm and a momentum thickness $\delta_\theta = 2.37$ corresponding to a Reynolds number $\mathrm{Re}_\theta = 3200$.

For the smooth edge configuration, the mean separation point takes place at $x/h = 2.17$ (Fig. 8a), while incipient and transitory detachments [1] occur at, respectively, $x/h > 1.8$ and $x/h = 2.24$, with a standard deviation $\sigma_{\mathrm{sep}} = 0.24$ h (Fig. 8c). The mean center of the recirculation zone locates at $\{x/h = 3.86;\ y/h = -0.74\}$, and the mean reattachment point at $x/h = 4.86$ (Fig. 8a). This results in a separation length $L_{\mathrm{sep}} = 2.7h$. As for salient-edge experiments, the maximum levels of TKE (Fig. 8b) localize in the shear layer. From the mean separation point to $x/h = 4.4$ ($y/h = -0.57$), TKE value progressively increases from $k/U_0^2 = 0.01$ to $k/U_0^2 = 0.03$. This maximal level is preserved up to $x/h = 5.45$, before decreasing as flow is going further downstream. The shear layer deflects toward the downstream flat plate, inducing an increase of the local pressure coefficient (Fig. 6, $x/h = 6$), which explains the decrease of TKE in the shear layer for $x/h > 5.45$.

The PSD of the transversal velocity component obtained by cross hot-wire measurement are shown in Fig. 9 for two positions: the first one in the shear layer near the separation point ($x/h = 2.5$) and the second in the wake flow ($x/h = 6$). Close to the separation point, the PSD presents a bump at a frequency of 70 Hz, corresponding to a Strouhal number

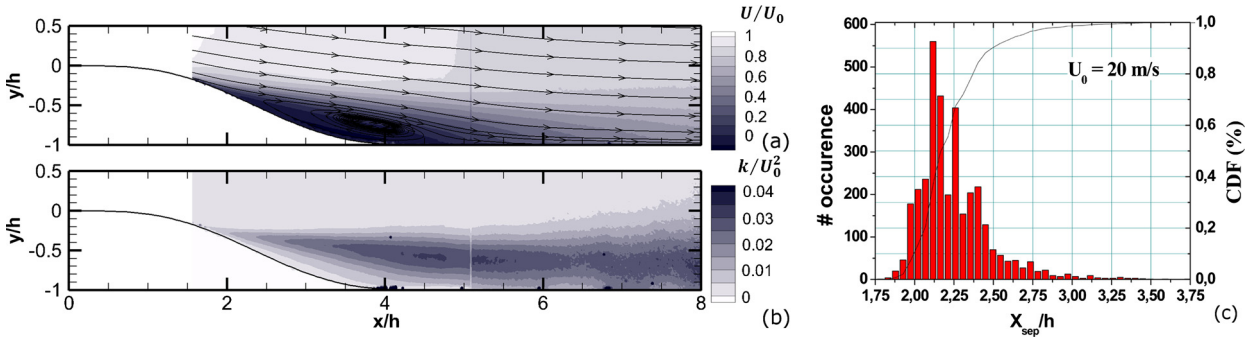

Fig. 8. (Color online.) (a) Mean streamwise velocity over the ramp, (b) TKE, (c) histogram and Cumulative Distribution Function of the unsteady position of the separation point.

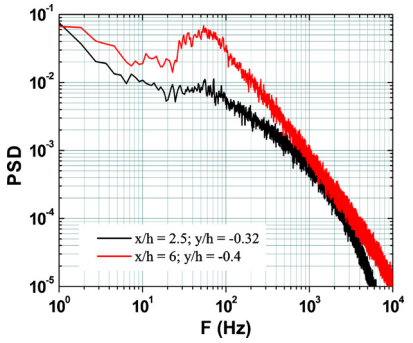

Fig. 9. (Color online.) PSD of transverse velocity component obtained in the shear layer near the separation point ($x/h = 2.5$) and in the wake flow ($x/h = 6$).

$\mathrm{St}_\theta = 0.010$ based on the momentum thickness of the boundary layer at $x/h = 0$. In the wake, a characteristic frequency of 30–50 Hz is observed, which gives a Strouhal number $\mathrm{St}_{L_{\mathrm{sep}}}$ between 0.4 and 0.67.

4. Conclusion

Salient edge ramp flow characterization shows that upstream from the separation point, the low favorable pressure gradient induces a TBL decreases. At the salient edge, the momentum thickness leads to a Reynolds number $\mathrm{Re}_\theta = 3780$ and a shear layer roll-up characterized by a Strouhal number $\mathrm{St}_\theta = 0.014$. The recirculation is characterized by a separation length $L_{\mathrm{sep}} = 5.3h$. The shear layer shows a high level of TKE, increasing up to the end of recirculation zone and a shedding frequency characterized by a Strouhal number $\mathrm{St}_{L_{\mathrm{sep}}} = 0.53$–$0.66$.

For the smooth-edge configuration, the TBL upstream from the separation point is first subject to a favorable pressure gradient, then to an adverse pressure gradient inducing a TBL separation at $x/h = 2.17$. The momentum thickness (at $x/h = 0$) Reynolds number is $\mathrm{Re}_\theta = 3200$ and scaled shear layer roll-up with a characteristic Strouhal number $\mathrm{St}_\theta = 0.010$. The separation length is $L_{\mathrm{sep}} = 2.7h$ and the shedding frequency of the shear layer presents a Strouhal number $\mathrm{St}_{L_{\mathrm{sep}}} = 0.4$–$0.67$.

Contrary to the salient edge configuration that presents a discontinuity, the progressive increase of pressure gradient for the smooth edge induces a delayed mean separation point and increases the fluctuations of the instantaneous separation point. As the separation point for the smooth edge occurs downstream from the separation point for the salient edge, the mean recirculation size is smaller. Furthermore, the shear layer deflects toward the downstream flat plate, which contributes to decrease the recirculation zone and the TKE.

The next step of this work will be devoted to active control with pulsed jet actuators as active vortex generator device. The analysis of the controlled flow depending on the actuation parameters will conduct us to highlight which instabilities are to be promoted for reducing the separated flow.

Acknowledgements

This work is part of the SePaCode Project funded by ANR France (ANR-11-BS09-018). The authors thank S. Loyer for technical support during the experiments.

References

[1] R.L. Simpson, Turbulent boundary-layer separation, Annu. Rev. Fluid Mech. 21 (1) (1989) 205–232.
[2] R.L. Simpson, Y.-T. Chew, B.G. Shivaprasad, The structure of a separating turbulent boundary layer. Part 1. Mean flow and Reynolds stresses, J. Fluid Mech. 113 (1981) 23–51.
[3] R.L. Simpson, Y.-T. Chew, B.G. Shivaprasad, The structure of a separating turbulent boundary layer. Part 2. Higher-order turbulence results, J. Fluid Mech. 113 (1981) 53–73.
[4] S. Song, D.B. Degraaff, J.K. Eaton, Experimental study of a separating, reattaching, and redeveloping flow over a smoothly contoured ramp, Int. J. Heat Fluid Flow 21 (5) (2000) 512–519.
[5] R. Mittal, R.B. Kotapati, L.N. Cattafesta, Numerical study of resonant interactions and flow control in a canonical separated flow, AIAA Pap. 1261, 2005.
[6] H. Tennekes, J. Lumley, A First Course in Turbulence, MIT Press, Cambridge, MA, USA, 1972.
[7] M.A.Z. Hasan, The flow over a backward-facing step under controlled perturbation: laminar separation, J. Fluid Mech. 238 (1992) 73–96.
[8] K. Zaman, A. Hussain, Turbulence suppression in free shear flows by controlled excitation, J. Fluid Mech. 574 (1981) 25–58.
[9] N.J. Cherry, R. Hillier, M.E.M. Latour, Unsteady measurements in a separated and reattaching flow, J. Fluid Mech. 144 (1984) 13–46.
[10] J. Dandois, E. Garnier, P. Sagaut, Numerical simulation of active separation control by a synthetic jet, J. Fluid Mech. 574 (1) (2007) 25–58.
[11] D.G. Mabey, Analysis and correlation of data on pressure fluctuations in separated flows, J. Aircr. 9 (1972) 642–645.
[12] M. Forte, A. Debien, D. Caruana, N. Benard, P. Barricau, C. Gleyzes, E. Moreau, Mid-chord separation control using PSJ and DBD plasmas actuators, ERCOFTAC Bull. 94 (2013).
[13] T. Shaqarin, C. Braud, S. Coudert, M. Stanislas, Open and closed-loop experiments to reattach a thick turbulent boundary layer, in: TSFP7, 28–31 July 2011, Ottawa, Canada, 2011, http://www.tsfp-conference.org/index.php/proceedings/22-tsfp7-contents-of-volume-3, http://www.tsfp-conference.org/images/stories/proceedings/2011/8c4p.pdf.
[14] W.L. Siauw, J.-P. Bonnet, J. Tensi, L. Cordier, B.R. Noack, L. Cattafesta, Transient dynamics of the flow around a NACA 0015 airfoil using fluidic vortex generators, Int. J. Heat Fluid Flow 31 (2010) 450–459.
[15] S.S. Collis, D.J. Ronald, A. Seifert, V. Theofilis, Issues in active flow control: theory, control, simulation and experiment, Prog. Aerosp. Sci. 40 (2004) 237–289.
[16] D. Greenblatt, I.J. Wygnansky, The control of flow separation by periodic excitation, Prog. Aerosp. Sci. 36 (2000) 487–545.
[17] M. Gad-el-Hak, The taming of the shrew: why is it so difficult to control turbulence? in: Active Flow Control, Springer, Berlin, Heidelberg, 2007, pp. 1–24.
[18] D. Arnal, Special Course on Stability and Transition of Laminar Flow, AGARD-R-709, 1984.
[19] P.H. Alfredsson, R. Örlü, The diagnostic plot—a litmus test for wall bounded turbulence data, Eur. J. Mech. B, Fluids 29 (6) (2010) 403–406.
[20] S. Tardu, T.V. Truong, B. Tanguay, Bursting and structure of the turbulence in an internal flow manipulated by riblets, Appl. Sci. Res. 50 (3–4) (1993) 189–213.
[21] L.H. Benedict, R.D. Gould, Towards better uncertainty estimates for turbulence statistics, Exp. Fluids 22 (2) (1996) 129–136.